

1
2
3
4
5
6
7
8
9
10
11
12

Modeling monthly and seasonal Michigan snowfall based on machine learning: A multiscale approach

Lei Meng¹ & Laiyin Zhu^{1*}

¹ Department of Geography, Environment, and Tourism, Western Michigan University, Kalamazoo, Michigan, USA.

* Corresponding Author

13 **Abstract:**

14

15 Snowfall has important significance in water resources management and disaster prevention
16 worldwide. Accurate prediction of both mean and extreme snowfall is challenging because of
17 multiple controlling mechanisms at different spatial and temporal scales. By using a 65 years long
18 in-situ snowfall observation, we evaluated seven different machine learning algorithms for
19 predicting monthly snowfall in the Lower Peninsula of Michigan (LPM). The Bayesian Additive
20 Regression Trees (BART) demonstrates the best fitting ($R^2 = 0.88$) and out-of-sample prediction
21 skills ($R^2 = 0.58$) for the monthly mean snowfall followed by the Random Forest model. The BART
22 also demonstrate strong predictive skills for seasonal and the extreme monthly snowfall. Both
23 machine learning models also demonstrate signals of key physical processes controlling the
24 snowfall including topography, local/regional environmental factors, and teleconnections.
25 Particularly, models with the non-parametric framework can incorporate signals from multiple
26 scales and nonlinear responses from the snowfall to environmental factors and that substantially
27 improved the model prediction skills. The multiscale machine learning approach provides a
28 reliable and computationally efficient alternative approach to predict/forecast weather and climate
29 and has potential to be applied to other extreme weather prediction scenarios.

30

31 **Keywords:** Snowfall, Monthly and Seasonal, Michigan, Machine Learning, Prediction

32

33

34 **1. Introduction**

35

36

37 Snowfall is an important indicator of winter season severity along with low temperatures,
38 freezing rain, winds, visibility in cold climates (Ford et al., 2021). Snowfall intensity, duration,
39 and amount could have both beneficial and adverse impacts on society and environment (Kenneth
40 E. Kunkel et al., 2002), forest ecosystem (Zhou et al., 2021), plant phenology (Bjorkman et al.,
41 2015), and hydrological processes (Kolka et al., 2010). The Lower Peninsula of Michigan (LPM)
42 in the US Midwest region (Fig. 1) experiences substantial amounts of snowfall during winter
43 seasons and frequent extreme snowstorms due to the lake-effect. It has been demonstrated that
44 snowfall variability in the LPM has increased, although long-term averaged snowfall remains
45 relatively stable since 1970s(Meng & Ma, 2021). Model outputs from the Sixth Coupled Model
46 Intercomparison Project (CMIP6) suggest that snowfall intensity will increase while the amount
47 of snowfall might decrease in middle latitudes of North America under future warming(Quante et
48 al., 2021). Understanding the variability of snowfall will improve its predictability at monthly to
49 seasonal timescales, providing potential benefits for winter road maintenance budget planning, ski
50 industry, insurance company, and human health conditions.

50

51

52

53

54

55

56

57

Previous studies have discussed different mechanisms influencing winter snowfall
variability in the Great Lakes regions, including both local/regional environmental factors and
teleconnections. Local/regional environmental factors influence snowfall developments in the
Great Lakes regions through their impacts on atmospheric instability, lift, and moisture exchanges
between the Great Lakes and the atmosphere. Similar upward trends in air temperatures (as a proxy
of lake surface water temperatures) and snowfall in the Laurentian Great Lakes were also identified
(K E Kunkel et al., 2009). It was also found that a strong negative correlation existed between
average winter temperatures and lake-effect snowfall in Lake Michigan (Braham & Dungey, 1984).

58 Our recent studies (Meng et al., 2021; Meng & Ma, 2021) and other previous research (Clark et
59 al., 2016) suggest that both the lake-effect snowfall and the seasonal total snowfall variability have
60 significantly negative correlations with regional average winter temperatures in the LPM. Lake
61 surface water temperatures and ice covers also have significant impacts on lake-effect snowfall
62 from lake-atmosphere interactions. For instance, Baijnath-Rodino et al. (Baijnath-Rodino et al.,
63 2018) suggested that that warm lake surface introduces boundary layer instability and facilitate
64 exchange of moisture and energy, which fuels the lake effect snow. Several regional modeling
65 studies (Notaro et al., 2013; Shi & Xue, 2019) support the same mechanism and describe the roles
66 of lake surface temperatures, ice coverage and wind directions in the development of lake-effect
67 snowfall with more details.

68 Teleconnections can determine the snowfall in the Great Lakes regions from mechanisms
69 at global or regional scales. For example, the upper-level trough patterns favorable to the lake-
70 effect snow are often associated with a negative phase of Arctic Oscillation (AO) and North
71 Atlantic Oscillation (NAO) and/or a positive phase of Pacific North American Pattern (PNA)
72 (Suriano & Leathers, 2017). Statistical model also shows that inclusion of the PNA, Pacific
73 Decadal PDO, Northern Hemisphere temperature and the NAO/AO improved the prediction skills
74 of snowfall in most stations in the United States (Kliver & Leathers, 2015). El Niño–Southern
75 Oscillation (ENSO) is controlling the snowfall in the Midwest U.S. by modulating the locations
76 of the jet stream (Smith & O’Brien, 2001). Significantly less snowfall has been observed during
77 El Niño (the warm phase of ENSO) years (Clark et al., 2016). Sea surface temperature in the Niño
78 3.4 region (SST3.4) are also negatively correlated with both seasonal total snowfall and lake-effect
79 snowfall in the LPM (Meng et al., 2021; Meng & Ma, 2021).

80 Based on the discussions above, most previous studies treat multiple mechanisms
81 influencing the regional snow separately, such as regional mechanisms like the lake-effect snow
82 or large-scale teleconnections such as ENSO. But these multiple atmospheric and environmental
83 factors are at different spatial and temporal scales and may determine snowfall LPM independently
84 or collectively. It is still challenging for the Global Circulation Models (GCMs) or Regional
85 Climate Models (RCMs) to capture all these mechanisms and both are currently computational
86 expensive (Gutowski et al., 2021). Machine learning approaches provide an alternative approach
87 to solve those multiscale challenges in weather and climate prediction. In recent years, machine
88 learning approaches have been more frequently used in parameterization of climate models
89 (O’Gorman & Dwyer, 2018; Schneider et al., 2017) or directly for regional and global climate
90 predictions (Ham et al., 2019). It has been reported that machine learning models are able to give
91 decent prediction skills for general climate variables like temperature and precipitation (Gibson et
92 al., 2021; Robertson et al., 2015). Those machine learning approaches are also demonstrating
93 improved ability to predict hydro-climate extremes, such as drought, extreme rainfall (Wei et al.,
94 2022). However, very few studies have used machine learning approaches to predict snowfall.
95 Non-linear autoregressive networks model was developed to enhance the spatial resolution of
96 snowfall estimate for the black forest using additional topographic information (Sauter et al., 2010).
97 The support vector machine (SVM) and multivariate discriminant analysis (MDA) models both
98 have excellent performance in snow avalanche prediction in the Karaj watershed, northern Iran
99 (Choubin et al., 2019). No machine learning based study is focused on a region like Michigan,
100 which is usually prone to extreme snowfall due to the lake-effect.

101 In this study, we will evaluate snow prediction models based on multiple machine learning
102 techniques. By doing this work, we will be able to (1) compare different machine learning

103 approaches for their fitting and prediction skills for snowfall in the LPM; (2) discover possible
104 important physical mechanisms that control LPM snowfall; (3) select an optimal model with best
105 predictive performance that can be used for seasonal/monthly forecast or future climate change
106 predictions.



107
108 **Fig. 1. Locations of all COOP stations with snowfall measurement in LPM.**

109
110 **2. Data and Methods**

111 **2.1 Snowfall and independent variables**

112 In this study, we use a monthly snowfall dataset from 8 COOP stations that are temporally
113 homogeneous (K E Kunkel et al., 2009). Only dataset from 1951 to 2015 is used due to constraints
114 of availability in the corresponding teleconnection indices. Only snowfall observations from the
115 peak snowfall season (December, January, and February) are included in our machine learning
116 models.

117 All independent variables are listed as Table 1. Vapor pressure deficit is the difference
118 between the actual water vapor pressure and saturation vapor pressure. Extreme temperature
119 (maxT & mint) and vapor pressure deficit (vpdmax & vpdmin) at each COOP station were
120 obtained from the nearest grid cell in the Precipitation-Elevation Regression on Independent
121 Slopes Model (PRISM) dataset^{53,54} with a 4 km spatial resolution. Extracted from the same data
122 source, both local and regional averaged temperatures (savgT & avgT) are included in our machine
123 learning models. uwind and vwind were obtained from the nearest grid cell in ERA5-land monthly
124 dataset with a 0.25° spatial resolution. The wind direction is calculated from uwind and vwind
125 values.

126

127 **Table. 1. List of variables used in the modeling process**

Acronym	Full name	Description	Unit
maxT	Maximum Temperature	Local, Dynamic	°C
minT	Minimum Temperature	Local, Dynamic	°C
savgT	Station Averaged Temperature	Local, Dynamic	°C
avgT	Regional Averaged Temperature	Regional, Dynamic	°C
rangeT	Range of Temperature	Local, Dynamic	°C
uwind	Meridional Winds	Local, Dynamic	m/s
vwind	Zonal winds	Local, Dynamic	m/s
direction	Direction of the winds	Local, Dynamic	°
vpdmax	Maximum Vapor Pressure Deficit	Local, Dynamic	kPa
vpdmin	Minimum Vapor Pressure Deficit	Local, Dynamic	kPa
tsi	Tropical Southern Atlantic Index	Teleconnections	°C
tni	Tropical Southern Atlantic Index	Teleconnections	°C
np	North Pacific Air Pressure	Teleconnections	mb
sst34	Sea Surface Temperature in Nino3.4	Teleconnections	°C
pna	Pacific North America Index	Teleconnections	NA
nhavgT	Average Temperature of Northern Hemisphere include both land and ocean	Teleconnections	°C
nao	North Atlantic Oscillation	Teleconnections	NA

pdo	Pacific Decadal Oscillation	Teleconnections	NA
ao	Arctic Oscillation	Teleconnections	NA
elev	Elevation	Local, Static	meter
dist2shore	Shortest Distance to Lake Michigan shorelines	Local, Static	Kilometer
lat	Latitude of Station	Local, Static	°
lon	Longitude of Station	Local, Static	°
month	Month of observation	Generic, Dynamic	NA

128 * All dynamic variables are extracted monthly

129

130 The selection of teleconnection indices used in the models is based on previous literature
131 showing their controls in snowfall in the U.S. (Clark et al., 2016; Hartnett et al., 2014; Kluver &
132 Leathers, 2015; Meng et al., 2021; Meng & Ma, 2021; Suriano & Leathers, 2017). All
133 teleconnection indices including tsi, tni, np, sst34, pna, nhavgT, nao, pdo, and ao were obtained
134 from NOAA Physical Sciences Laboratory (PSL, <https://psl.noaa.gov/data/climateindices/list/>).
135 Latitude, longitude, elevation, and the shortest distance (in km) to Lake Michigan shorelines for
136 each COOP station were also included in our models and they do not change by time in the model
137 (static variables). The u and v component of the surface wind were collected from ERA5 data (Bell
138 et al., 2021). Wind direction is calculated from the corresponding u - and v -winds at each grid cell.

139

140 2.2 Model Overview

141 We tested 7 different algorithms that cover major categories of machine learning
142 techniques in this study. The Generalized Linear Model (GLM) are a series of special linear
143 regression models first formulated by Nelder and Wedderburn (1972). They work for the situation
144 when the response variable is reacting nonlinearly with predictors by using a link function (such
145 as logarithm function) to allow variance of each measurement to be a function of its prediction.
146 The Generalized Additive Model (GAM) is a special kind of GLM where the response variable is

147 linearly dependent on smooth functions of some predictor variables (Sasieni, 1992). An
148 exponential distribution is specified for the response variable and the predictor variables is linked
149 with smooth functions such as polynomial, spline or nonparametric functions.

150 The Bayesian Regularization for Feed-Forward Neural Networks (BRNN) is a two-layer
151 framework of neural network that uses the Nguyen and Widrow Algorithm (Nguyen & Widrow,
152 1990) to assign initial weight and Gauss-Newton algorithm to perform the optimization. It has
153 been applied to predicting complex quantitative genetic traits (Gianola et al., 2011) and is first
154 applied to climate prediction models in our analysis.

155 The Supporting Vector Machine (SVM) is a machine learning algorithm that discover an
156 optimal hyper plane that classifies the data points from a multi-dimensional space (Boser et al.,
157 1992). It already has been applied to climate science, such as prediction of extreme rainfall event
158 (Nayak & Ghosh, 2013) and downscaling precipitation from GCMs (Tripathi et al., 2006). Those
159 predictions both show good agreements with observations so here we include the SVM in our
160 model comparison.

161 The Multivariate Adaptive Regression Splines (MARS) is a non-parametric modeling
162 approach that can model the nonlinearities and interactions in the data without knowing them *a*
163 *priori* (J. H. Friedman, 1991). This algorithm acts as an expansion of product spline basis functions,
164 where the number of functions and their parameters are automatically determined by the data. The
165 MARS has been successively applied to predict monthly runoff in tropical climate (Reddy et al.,
166 2021) and burn area from wildfire in western boreal North America (Balshi et al., 2009).

167 The Random Forest (RF) and Bayesian Additive Regression Trees (BART) are both machine
168 learning algorithms based on ensembles of decision trees. The RF constructs multiple decision

169 trees and its mean prediction is given by those trees (Breiman, 2001). This approach is believed to
170 be able to provide more robust predictions and suffer from less overfitting to the training set as
171 compared with single decision tree. The BART algorithm is another “sum-of-trees” based model
172 where each tree starts with constrain as a weak learner, then the fitting and inference are finished
173 by using iterative Bayesian backfitting MCMC algorithm creating samples from a posterior
174 (Chipman et al., 2012). The BART adds the Bayesian prior-posterior framework in the ensemble
175 tree modeling. And its predictive performance is proved better than boosting, the lasso, MARS,
176 neural nets, and the RF with even less computation resources. We will test both RF and BART for
177 our snowfall modeling.

178 **2.3 Model evaluation and selection**

179 We start our modeling by splitting our data randomly into 80% training data and 20%
180 testing data. The classification and regression training (caret) R package (Kuhn, 2008) is used to
181 select the optimal combination of variables for each model in the model training by using the
182 included Recursive Feature Elimination (RFE) function. For example, the RFE use stepwise
183 feature selection for the GLM model and use cross validated recursive variable selection for GAM,
184 SVM, MARS, RF, and BART. There is no variable selection for BRNN. The RFE test all possible
185 combinations of variables into the model, evaluate their cross-validation results (RMSE, R^2 , and
186 MAE from 10-folds cross validation), and finally select the model with the best results. We will
187 train those models using the selected variables and compare the model fitting results for all 7 those
188 algorithms.

189 The next step is to use the 20% testing data to execute the out of sample cross validation
190 to test the models’ sensitivity and robustness to new data. We will use the identical models trained
191 from the previous step to make predictions for the snowfall observations in the testing data and

192 make comparisons. The RMSE, MAE, and R^2 will be calculated to gauge different models' out of
193 sample prediction skills. We will choose one or two machine learning algorithms with the best
194 prediction skills for further evaluation, which will be the hold-one-year-out cross validation. The
195 purpose is to test models' sensitivity and stability in predicting seasonal snowfall in LPM. We will
196 iteratively hold out each year's data and train the model only with other 64 years. Each hold-out
197 model will be used to predict monthly snowfall at each station for that hold-out year. Monthly
198 predictions and observations will be both aggregated seasonally (three months) and compared.

199 One of the major challenges for all machine learning research is model interpretation
200 (Molnar et al., 2020). Model interpretation will help identify important variable/physical process
201 involved in the machine learning model and understand how the dependent variables are
202 interacting with independent variables. We will be able to calculate the variable importance for
203 different machine learn approaches used in this study(Grömping, 2009). For example, the t-statistic
204 for each model parameter is used for GLM. The reduction (addition) to the model performance
205 (such as residual sums of squares) when a predictor is added to (removed from) the model is
206 calculated as the importance of each predictor for models including MARS, RF, and BART. For
207 better comparison purposes, we will calculate the relative variable importance (VI) relative VIs
208 based on a 0–100 scale for model comparison purposes. Finally, the Partial Dependence Plot (PDP)
209 is a useful tool to demonstrate the marginal effect from one or two predictors to the predicted
210 outcome (Jerome H. Friedman, 2001). We will be able tell how snowfall is reacting to one specific
211 predictor (e.g., linearly or non-linearly) in the model. Combining the VI and PDP calculation, we
212 expect to reveal important physical mechanisms that control snowfall in the LPM.

213
214
215
216

3. Results

217 **3.1 Linear Correlations**

218

219 Linear correlations between all monthly snowfall and environmental/climatological factors

220 are shown in Table 2. Maximum temperature (maxT) has the highest correlation with the snowfall

221 in the LPM, followed by the regional averaged temperatures (avgT). Both the maxT and avgT

222 have a strong negative correlation with the snowfall. Station’s geographical locations also have an

223 impact on the amount of snowfall. More snowfall is associated with stations with shorter distance

224 from the Lake Michigan and locations with higher latitudes tend to have more snowfall. Most of

225 the teleconnections have weak or no statistically significant correlation with the snowfall. Two

226 strongest signals are SST 3.4 and North Atlantic Oscillation.

227 **Table 2. Linear correlations between Michigan snowfall and independent variables**

month	lon	lat	elev	dist2shore	ao
-0.1*	-0.004	0.32*	-0.25*	-0.24*	0.03
nhavgT	np	pdo	pna	sst34	nao
-0.01	0.04	-0.07	-0.05	-0.14*	-0.11*
avgT	tni	tsi	savgT	minT	maxT
-0.36*	0.05	0.08	0.06	-0.26*	-0.42*
rangeT	uwind	vwind	direction	vpdmax	vpdmin
-0.09	0.26*	-0.19*	0.18*	-0.11*	-0.03

228 * Indicates statistically significant correlation at 99% level

229

230 **3.2 Model fitt**

231 The correlation analysis provides information about snowfall’s linear response to individual

232 predictors. In this section, we will evaluate seven different machine learning algorithms to explore

233 their combined effect. We used the Recursive Feature Elimination (RFE) algorithm to test all

234 possible combinations of predictors and chose the optimal combination (statistics shown as SI. 1-

235 5). The number of required variables for the best fitting models varies from 4 to all independent

236 (24) variables. Significant differences exist in the model fitting accuracy among the seven

237 algorithms (Table 2). The R^2 varies from 25% (SVM) to 88% (BART). The BART model also has
 238 the lowest mean absolute error (MAE) and Root Mean Square Error (RMSE), followed by the RF
 239 model.

240 The VI rankings also show differences among seven machine learning algorithms (Table 3).
 241 Similar to the correlation analysis, maxT is the most important controlling variable in GLM,
 242 MARS, SVM, and RF and the third important variable in BART. avgT is another important
 243 variable in many machine learning models (ranked second in GLM, SVM, and RF). Elevation is
 244 an important static variable along with the latitude, which appears in the top 10 VIs of most models
 245 except the SVM. For the BART with the best fitting performance, the top 5 important variables
 246 are vpdmax, dist2shore, maxT, rangeT, and elevation.

247

248 **Table 2. The Model fitting result for the 80% training data**

	GLM	GAM	BRNN	SVM	MARS	RF	BART
Number of Predictors	24	19	24	4	10	17	24
R^2	0.4	0.42	0.45	0.25	0.44	0.58	0.88
MAE	18.11	18.03	18.03	19.76	17.58	15.29	8.48
RMSE	23.95	23.52	23.11	26.97	23.01	20.24	11.07

249

250

251

252

253

254

255

256

257

258

259

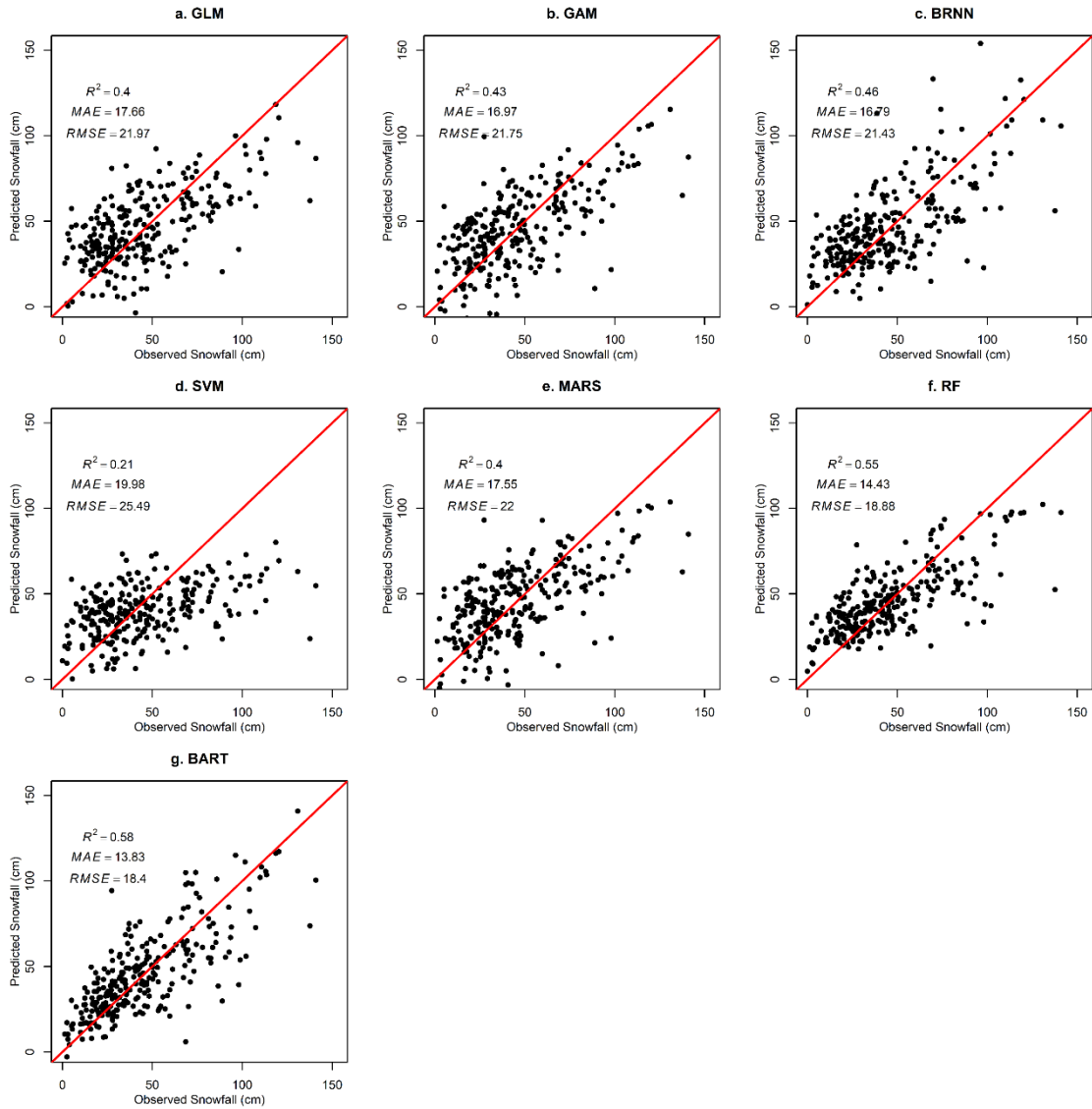
260 **Table 3. Relative variable importance (VI) for different ML algorithms (only up to 10 most**
 261 **important variables are shown).**

Rank	GLM		GAM		MARS		SVM		RF		BART	
	Var	VI	Var	VI	Var	VI	Var	VI	Var	VI	Var	VI
1	max T	100	lat	100	max T	100	max T	100	max T	100	vpdm ax	100
2	avgt	69	mont h	99	elev	76	avgt	78	avgt	70	dist2 shore	97
3	minT	55	elev	87	mont h	54	minT	55	minT	61	max T	97
4	lat	54	pdo	86	dist2 shore	46	lat	54	dist2 shore	42	range T	90
5	uwin d	32	avgt	74	pdo	40			elev	42	elev	89
6	direct ion	31	minT	64	tsi	32			lat	27	tsi	88
7	elev	27	t1	60	vpdm ax	25			vpdm ax	25	avgt	85
8	dist2 shore	23	range T	45	np	22			range T	24	np	82
9	vwin d	22	tni	39	pna	16			t	23	lat	73
10	t	16	np	34	minT	13			np	22	vwin d	72

262

263 3.3 Cross Validation

264 Next, we used those trained models to make out-of-sample predictions using the 20% testing
 265 data (Fig. 2). Comparison of model predictions demonstrates that most models are robust and have
 266 stable prediction skills for the new data. BART has the best prediction skills, followed by RF,
 267 BRNN, GAM, GLM, MARS, and SVM, based on their MAE and RMSE statistics. BART has a
 268 $R^2 = 0.58$ with $RMSE = 18.4$ and $MAE = 13.83$. The RF Model's prediction skill is slightly lower
 269 than BART, with $R^2 = 0.55$ and $MAE = 14.43$. Particularly, the BART model has the best prediction
 270 skill for the > 100 cm snowfall. Most other models (GLM, GAM, SVM, MARS, and RF) tend to
 271 have systematic underestimate for this range of extreme snowfall. BRNN (Fig. 2c) have both large
 272 overestimates and underestimates for the > 100 cm snowfall.



273

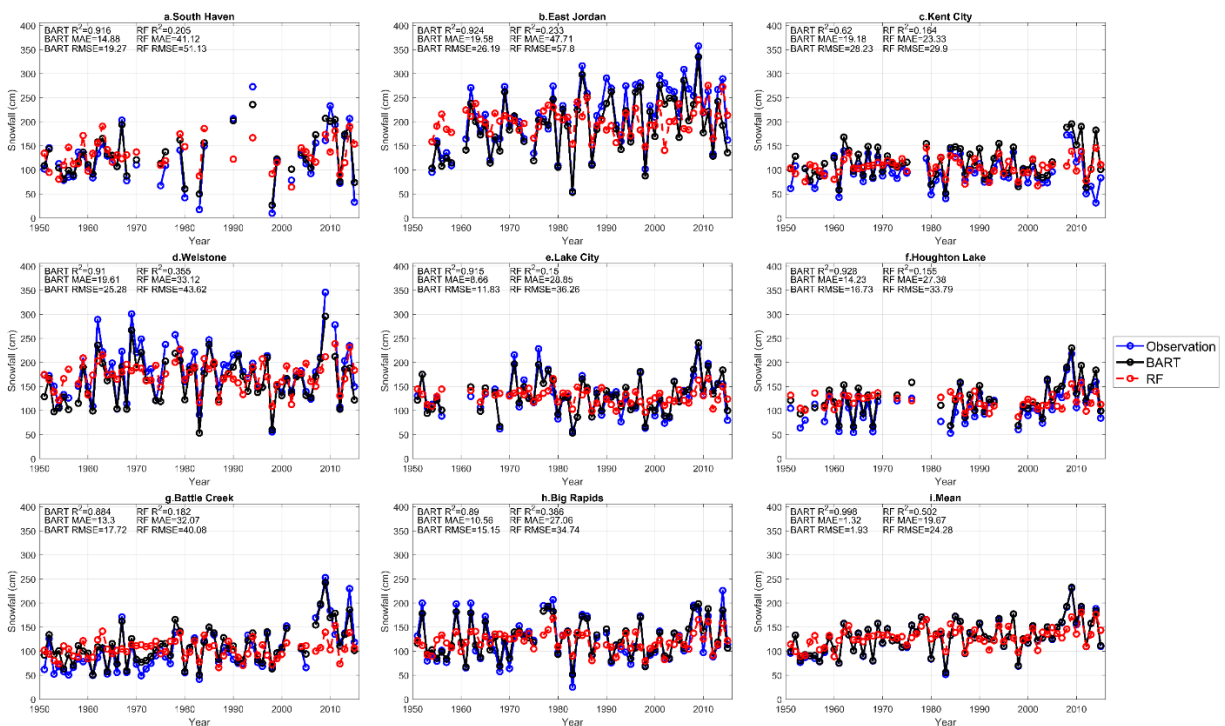
274 **Fig 2. The model prediction skills for different ML algorithms, calculated from the out-of-**
 275 **sample cross validation using the 20% testing data. Prediction and observation (same 20%**
 276 **testing data) are compared with the y=x line (red).**

277

278 We further evaluated model performances through the leave-one-year-out-cross validation
 279 for BART and RF because they have the best performance shown by the fitting and out-of-sample
 280 cross-validation tests. Fig. 3 shows that BART model can explain 62% to 92.4% of seasonal
 281 snowfall variance (summed as Dec, Jan and Feb) while RF can explain 15% to 38.6% of seasonal
 282 snowfall variance in the LPM as indicated by their R^2 . When the snowfall predictions are averaged

283 over the 8 stations, there is a significant improvement in model prediction skills and error statistics
 284 (Fig. 3i). The BART model demonstrates an exceptional high R^2 value of 99.8% and low values
 285 of MAE (1.32 cm) and RMSE (1.96 cm) for the station averaged regional snowfall prediction. The
 286 Random Forest model also shows improvement in predicting regional mean snowfall ($R^2 = 0.5$,
 287 MAE = 19.67) as compared with the single station prediction. Besides inter-annual and inter-
 288 decadal variability, both RF and BART also capture temporal trends at some locations' time series
 289 (Such as East Jordan, Battle Creek, and the Regional Mean)

290
 291



292
 293 **Fig 3. Hold one year out cross validation results for RF and BART models. For each year,**
 294 **both model (RF and BART) are trained only using data exclusively from other 64 years.**
 295 **Each hold-out model is used to predict snowfall monthly snowfal at each station and then**
 296 **they are aggregated into the seasonal snowfall as shown by the time series.**

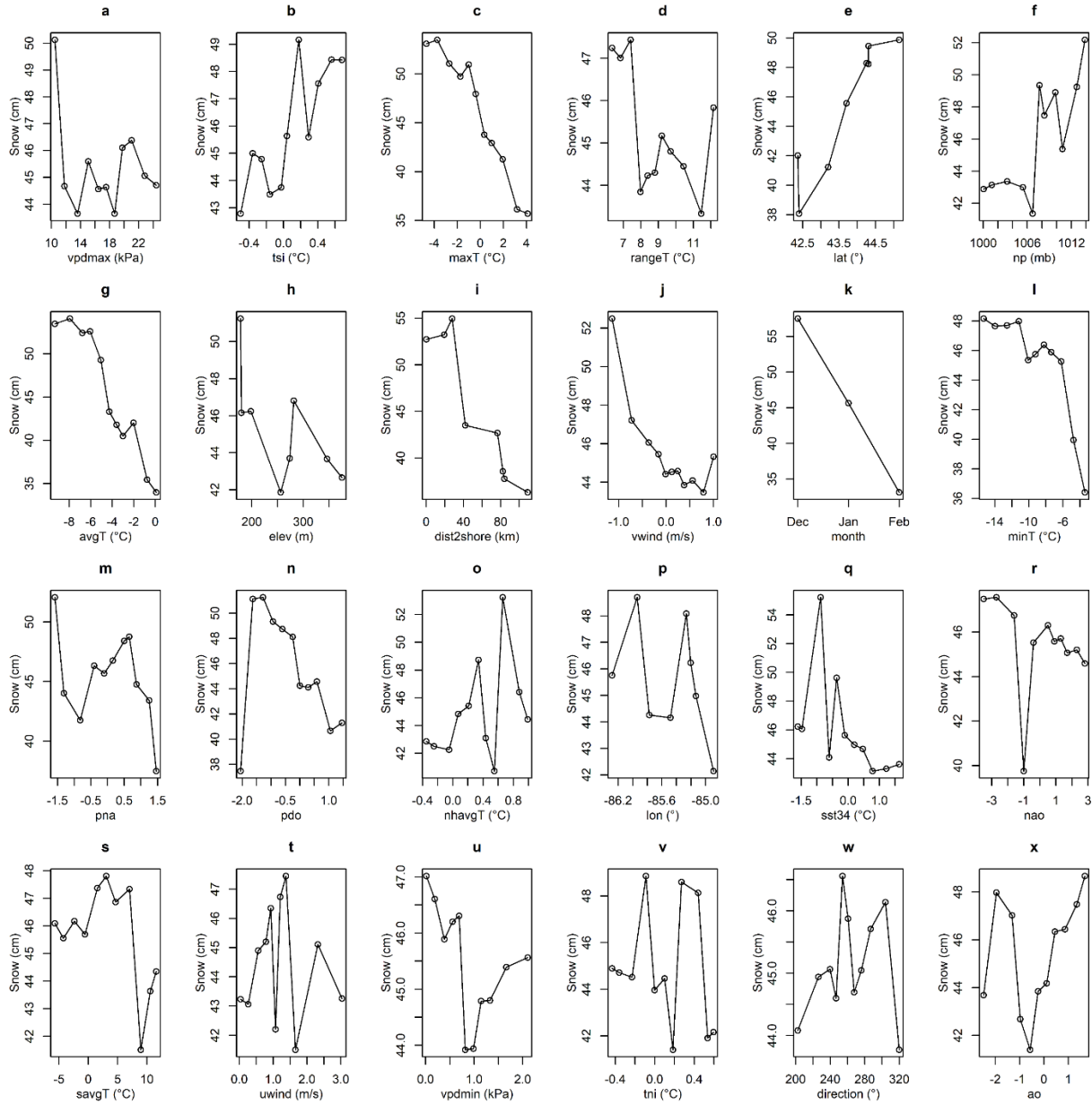
297

298 3.4 Variable and Model Interpretations

299 The partial dependence plots (pdps) can be used to estimate each dependent variable's
300 marginal effect on the predicted outcome of a machine learning model (Jerome H. Friedman, 2001).
301 The pdps for BART (Fig. 4) shows that snowfall generally increases as maxT, minT and avgT
302 decreases. This agrees with the correlation analysis and previous studies (Meng et al., 2021; Meng
303 & Ma, 2021) . The air temperature is likely to influence the rate of accretion of ice and
304 sublimation/deposition of snow as well as the mean size of snow aggregate (Hong et al., 2004).
305 The snowfall reacts to station mean temperature (savgT) in a more complex way. While the
306 snowfall generally decreases when the savgT increases in the BART (Fig 4s), the maximum
307 snowfall happens when the savgT is between 0 and 5 °C. And the RF demonstrate a positive
308 relationship between snowfall and savgT (Fig. 5i). At a much larger scale, higher north hemisphere
309 average temperature (nhavgT) generally agree with higher amount of LPM snowfall in both
310 models (Fig 4o and 5o). This could be related to the breaking down of polar vortex due to the
311 melting of arctic sea ice (Francis & Vavrus, 2012) or the general warm up of water temperature
312 that may intensify the lake-effect snow.

313 Static variables such as latitudes, dist2shore and elevation also play important roles in both
314 RF and BART. Snowfall is generally higher at locations nearer to the lakeshore (Fig 4i and 5d)
315 and locations with higher elevations (Fig 4h). This also agrees with the correlation analysis and
316 indicates signals from lake-effect snow because the process is directly determined by the
317 proximity to the great lakes and topography. Snowfall increases as the station's latitude
318 increases in both BART (Fig 4e) and RF (Fig 5f). The relationship is also controlled by
319 temperature's influence in snowfall.

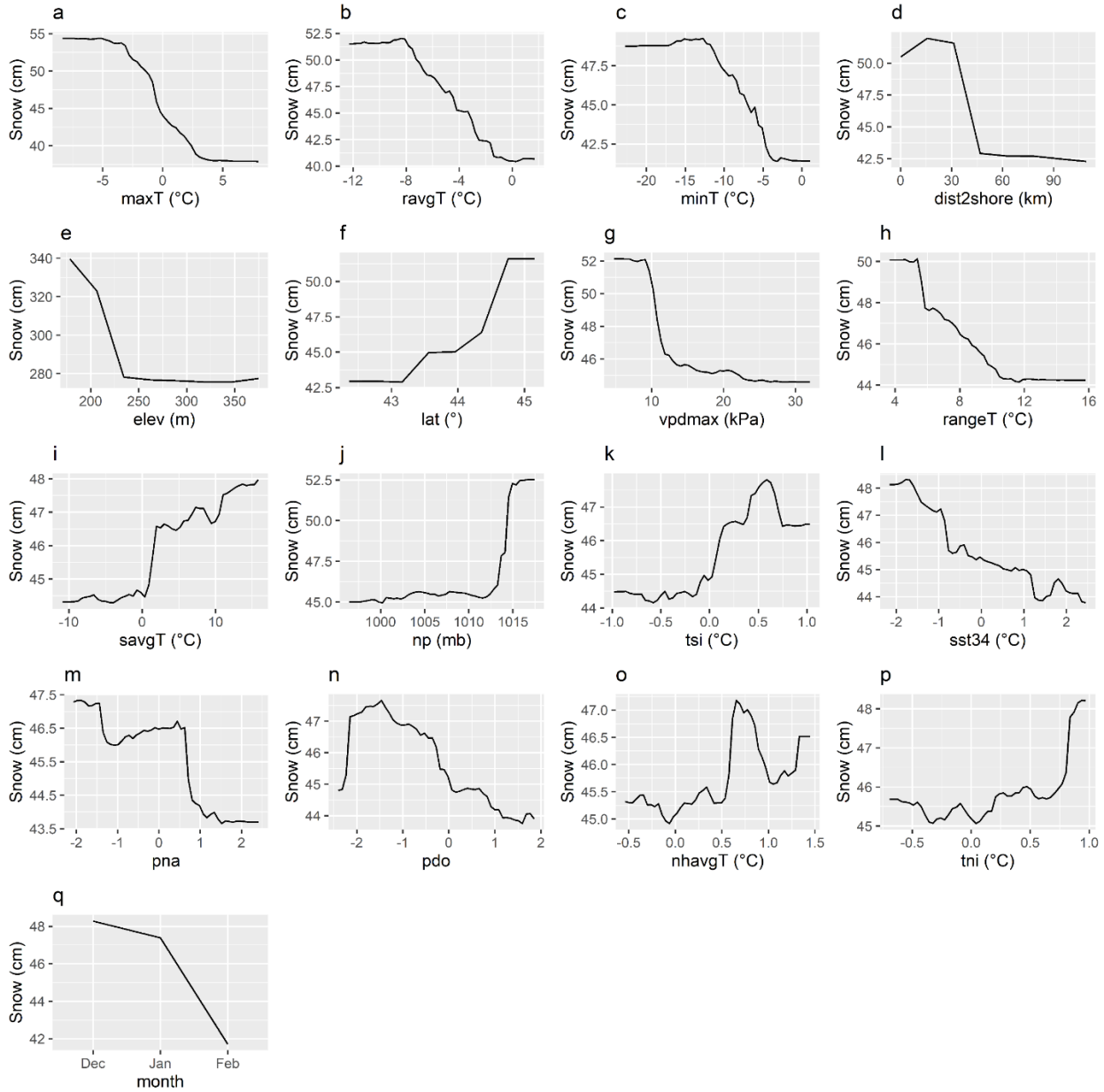
320 More snowfall amounts in the LPM are associated with the cold phase of ENSO (La Niña).
321 Previous studies have discussed how ENSO regulates the Pacific jet stream and therefore influence
322 the storm tracks over the continental U.S.(J. Chen & Kumar, 2002; Trenberth & Guillemot, 1996).
323 During the cold phase (La Niña), positive precipitation anomalies have been observed in
324 Washington, Oregon, and southwestern Canada (J. Chen & Kumar, 2002). Such negative
325 correlation has also been identified by recent studies on winter snowfall in Michigan (Meng et al.,
326 2021; Meng & Ma, 2021). Here both BART (Fig 4q) and RF (Fig 5l) models show ENSO's
327 controls in snowfall amount, while more nonlinearity is demonstrated by BART's relationship.
328



329

330 **Fig. 4** The partial dependence plot (pdp) for the BART model developed by 80% training
 331 **data**

332



333

334 **Fig. 5** The partial dependence plot (pdp) for the RF model developed by 80% training data,
 335 the pdp shows how the dependent variable changes with each predictor used in the model.

336

337 BART's pdps also demonstrate that the maximum vapor pressure (vpdmax) (Fig 4a) has
 338 a nonlinear relationship with snowfall. More snowfall is generally corresponding to < 14 kPa
 339 vpdmax. The vpd describes the difference between the amount of moisture in the air and the
 340 saturated moisture in the air. It is another measurement of relative humidity and has been applied

341 for estimating evapotranspiration (ET) in vegetations (Novick et al., 2016) and predicting the
342 wildfire (Chiodi et al., 2021). In our case low vapor pressure deficit values (< 14 kPa)
343 corresponds to high amount of atmospheric water vapor, which is favorable to the nucleation
344 process in all kinds of precipitation including snowfall. The snowfall remains fluctuated when
345 $vpd > 14$ kPa and demonstrates two small peaks when the vpd_{max} is at ~ 14.5 kPa and ~ 21 kPa
346 (Fig. 4a). In the RF model, vpd_{max} relationship has the same direction but with less nonlinearity
347 (Fig 5g). Interestingly, the BART model shows that higher snowfall is associated with weak
348 v_{wind} from the north (negative anomaly) and the wind direction from 250° to 310°
349 (northwesterly). During the winter, the North American High transports cold air from the north
350 and interacts with the warm air from the south to form synoptic winter storms. The cold air also
351 interacts with the warm lake surface to form lake effect snow in Michigan. This process is also
352 controlled by the ENSO intensity. For example, La Niña winter is associated with displaced
353 Polar jet to the great plains (Smith & O'Brien, 2001) and cooler/wetter winter in the upper
354 Midwest U.S. (Budikova et al., 2022).

355 Besides the ENSO, several other teleconnection indices also show different influences on
356 LPM snowfall in BART and RF models. The North Pacific index (np) is calculated as the area-
357 weighted sea level pressure over the North Pacific (Trenberth & Hurrell, 1994). The np is closely
358 related to the tropical and subtropical SST through ocean-atmosphere interactions and it also
359 interacts with the ENSO cycle. We show that snowfall amounts significantly increase when the np
360 is above 1006 millibars. This agrees with Chen and Song (2018) which shows significant negative
361 relationships between np and temperature in central Canada and U.S great lakes. The PDO reflects
362 remote changes of SST in the North Pacific and the sea level pressures over the Aleutian Island
363 (Mantua et al., 1997; Newman et al., 2016), which has teleconnections with winter temperature

364 and precipitation pattern in large portion of Midwest U.S. Both BART and RF pdps demonstrate
365 that the snowfall generally increases when the PDO anomaly is negative. Previous studies also
366 indicates that negative phases of PDO are normally associated with above normal winter
367 precipitation in a large portion of interior U.S. (Mantua et al., 1997; Newman et al., 2016). The
368 PNA is a changing pattern of SST and sea level pressure in the Pacific associated with ENSO but
369 also with atmospheric internal variability and SST anomalies (Li et al., 2019). It has strong
370 influence on precipitation in North American by modifying Polar jet flows and associated storm
371 tracks. Negative PNA phases are usually more favorable to northern displacement of jet over the
372 eastern U.S. It frequently causes intruding of maritime tropical air from the Gulf (Budikova et al.,
373 2022; Leathers et al., 1991) and enhancement in local precipitation in the eastern U.S. The pdps
374 (Fig 4m & Fig 5m) are showing similar patterns, where negative PNA anomalies are generally
375 associated with more LPM snowfall. The BART's PNA pdp has more nonlinearity than the RF
376 with a spike of snowfall increase when the PNA value is between -0.8 and 0.5 (Fig. 4m).

377 The Tropical Southern Atlantic Index (tsi, Fig 4b) is showing a general positive relationship
378 with the snowfall and this is a new relationship we have discovered from the model. The tsi is
379 closed related to the NAO on interannual to decadal time scales (Marshall et al., 2001). Such
380 relationship might be related to the existing linkage between snowfall and NAO. The NAO and
381 AO signals are closely related and they both control the upper-level winds and the polar vortex in
382 the Northern Hemisphere (Budikova et al., 2022). Positive NAO/AO phases are associated with a
383 stronger polar vortex that locks the cold air in the higher latitude while negative NAO/AO is
384 usually associated with enhanced meandering of polar jet and outbreaks of colder air into the lower
385 latitude (Budikova, 2012). This cold air usually introduces extreme low temperature and snowfall
386 (Ghatak et al., 2010). The NAO/AO only appear in the BART model with minor variable

387 importance. Fig 4r shows that higher snowfall is generally associated with negative NAO but its
388 relationship with AO is more complex (Fig 4x).

389

390 **3.5 Extreme snowfall**

391 Our results have clearly shown that BART and RF are the two best models for predicting
392 snowfall in the LPM. To evaluate their performance in predicting extreme snowfall events and
393 examine important factors, we selected the upper 30% ($> 70^{\text{th}}$ percentile) of the snowfall data to
394 develop two new BART and RF models. Results (Table 4) show that both extreme models have
395 decreases in their fitting skills as compared with those general models trained by the 80% randomly
396 selected sample (Table 3). The R^2 for RF has changed from 0.58 to 0.30 (-48%) while the R^2 for
397 BART has changed from 0.88 to 0.63 (-28%). The RF's RMSE increased from 20.24 to 21.06
398 (+4%) and MAE increased from 15.29 to 15.93 (+4%), while the BART's RMSE increased from
399 11.07 to 15.29 (+38%) and MAE increased from 8.48 to 11.53 (+36%). Therefore, the RF has
400 larger relative changes in R^2 while the BART has larger relative changes in RMSE and MAE.
401 Meanwhile, the BART model still performs better than the RF model with higher R^2 , lower MAE
402 and RMSE.

403 **Table 4. Fitting statistics for RF and BART models based on the upper 70 percentile of**
404 **snowfall data (extreme snowfall)**

Model	RMSE	R^2	MAE
RF	21.06	0.30	15.93
BART	15.29	0.63	11.53

405

406 In terms of VIs, both RF and BART extreme models show slightly differences from the general
407 models (Table 5). It is interesting to note that maxT and vpdmax are the two most important
408 predictors for both extreme models (Table 5). More snowfall is corresponding to lower maxT as

409 well as lower vpdmax (Fig 6), which are similar to their relationships shown by the regular models.
 410 Note that fluctuations in snowfall in higher range of vpdmax in Fig 4a disappear in Fig 6b,
 411 indicating a more dominate control of higher atmospheric moisture in generating extreme snowfall
 412 events. Other temperature variables (rangeT, avgT, minT) are also important in both RF and BART
 413 models for the extremes. And they all show negative relationships with the snowfall. The np is the
 414 only teleconnection variable that shows in the top 10 VI list for both RF and BART (Table 5). In
 415 Fig 6 and SI 6, we also find that the np and other teleconnection variables (ENSO, PDO, NAO,
 416 AO, and PNA) follow their relationship with the LPM snowfall in general models (Fig 4&5). The
 417 tsi has a positive relationship with snowfall in pdps for both BART (Fig 6d) and RF (SI 6i).

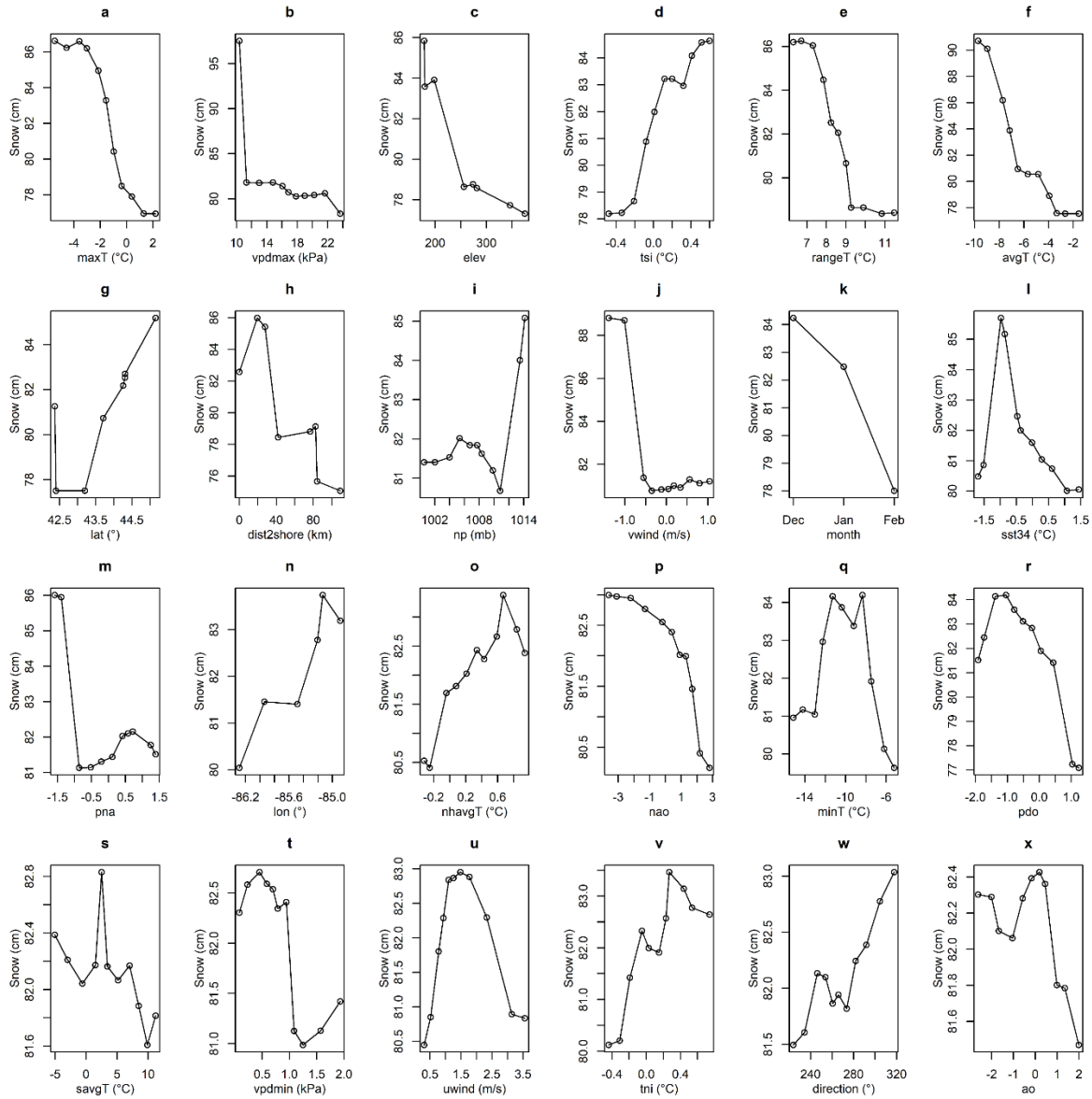
418 Many previous studies have mentioned that climate extremes prediction is challenging
 419 from both Earth System Models and Machine Learning models (Sillmann et al., 2017; Zhu &
 420 Aguilera, 2021; Zwiers et al., 2013). Our result shows that the RF and BART models both have
 421 slight degradations in their fitting skills for modeling extreme snowfall observations. They still
 422 can offer decent amount of explained variance (R^2), relatively small error statistics based on the
 423 extreme snowfall observations containing much larger variability and uncertainty. It can be also
 424 referred from the above analysis that the BART model overall does a reasonable job in the
 425 prediction of overall and extreme snowfall events in the LPM.

426

427 **Table 5. Relative variable importance (VI) for the 70 percentile models RF and BART**

Rank	RF		BART	
1	maxT	100	maxT	100
2	vpdmax	93	vpdmax	98
3	rangeT	85	elev	94
4	avgT	84	tsi	87
5	minT	68	rangeT	86
6	np	67	avgT	83

7	elev	64	lat	80
8	dist2shore	62	dist2shore	76
9	savgT	62	np	75
10	lat	52	vwind	73



429

430 **Fig 6. The partial dependence plot (pdp) for the BART model developed by the 70**
 431 **percentile data**

432

433

434 **4. Discussion and conclusion**

435 Our analysis suggests that temperatures are one of the most important predictors in machine
436 learning techniques predicting snowfall in the LPM. At each station, maximum and minimum
437 temperatures have a stronger impact on snowfall than the average temperatures. This indicates that
438 snow formation process in this region is more sensitive to extreme temperatures. Similar results
439 were found over the Canadian domain of the Great Lakes basin (Bajinath-Rodino et al., 2018). At
440 the global level, the north hemisphere averaged temperatures demonstrate negative relations with
441 the LPM snow. Physical mechanisms for this relationship such as polar vortex break or increased
442 temperature difference between lake surface and air need further investigations (Agee & Hart,
443 1990; Meng & Ma, 2021). The moisture availability is another important factor in both BART and
444 RF models and they generally show negative relationships with the snowfall. We need process
445 based Regional Climate Models (RCM) to understand more details about how the changing
446 temperature and water vapor in the atmosphere determine the lake-effect snow through lake-land-
447 atmosphere interactions and other synoptic processes.

448 Our models also demonstrate that latitude, elevation, and distance to shoreline are
449 important predictors for snowfall. The importance of these variables is possibly associated with
450 regional physical processes that lead to the development of lake-effect snowfall events. Elevation's
451 control in snowfall amounts in the Great Lakes region has been mentioned in previous literatures
452 (Hill, 1971; Niziol, 1987). RCM simulations also suggest that both annual snowfall and frequency
453 (days per year) decreases as the downwind distance from the Great Lakes increases (Notaro et al.,
454 2013). Inclusion of these local static variables has greatly improved the prediction skill of our
455 machine learning models.

456 Seven teleconnection indices, including NP, SST34, PNA, NAO, PDO, TNI, and AO, were
457 included in our snow prediction models. Machine learning techniques have no assumption of non-
458 collinearity among independent variables. Therefore, these teleconnections can work together to
459 improve the model prediction skill. Our results demonstrate several important teleconnection
460 indices in the snow prediction models, including SST34, PDO, and NP. These indices have non-
461 linear or linear relationships with snowfall in the LPM. Further investigations are needed to
462 validate the physical process reflected by those relationships shown by the machine learning
463 models. Particularly, we need to improve understanding the partition of snowfall into lake-effect
464 and non-lake effect snowfall in the Great Lakes regions because these two different types of
465 snowfall are produced through different physical mechanisms (Pettersen et al., 2020).

466 Our comparison of various machine learning models suggests the BART model can predict
467 mean and extreme monthly LPM snowfall with high accuracy. The machine learning approach
468 assimilates dynamic atmospheric/oceanic signals from multiple scales and static environmental
469 variables such as topography and distance to shore. It provides a reliable and computational
470 efficient alternative to current numerical weather/climate predictions (Chantry et al., 2021) as well
471 as a new way to identify possible physical mechanisms. In the future, the machine learning models
472 can be tested for other snow prone regions and used for predicting regional snowfall variability
473 and changes based CMIP climate projections for the future.

474

475 **Acknowledgments:**

476 L.M and L.Z are both supported by the Publication of Papers and Exhibition of Creative Works
477 (PPP&E) from the Western Michigan University.

478

479 **Author Contributions:**

480 L.Z. conceptualized and designed the research. L.M. and L.Z. executed the data analysis and
481 drafted the manuscript. L.M. and L.Z. edited the manuscript.

482

483 **Competing Interests statement**

484 The authors declare no competing interests.

485

486 **Data and materials availability:**

487 All data, code, and materials used in the analyses will be available from the authors upon
488 request.

489

490

491

492

493

494

495 **References**

- 496
- 497 Agee, E. M., & Hart, M. L. (1990). Boundary layer and mesoscale structure over Lake Michigan
498 during a wintertime cold air outbreak. *Journal of the Atmospheric Sciences*, 47(19).
499 [https://doi.org/10.1175/1520-0469\(1990\)047<2293:BLAMSO>2.0.CO;2](https://doi.org/10.1175/1520-0469(1990)047<2293:BLAMSO>2.0.CO;2)
- 500 Baijnath-Rodino, J. A., Duguay, C. R., & LeDrew, E. (2018). Climatological trends of snowfall
501 over the Laurentian Great Lakes Basin. *International Journal of Climatology*, 38(10).
502 <https://doi.org/10.1002/joc.5546>
- 503 Balshi, M. S., McGuire, A. D., Duffy, P., Flannigan, M., Walsh, J., & Melillo, J. (2009).
504 Assessing the response of area burned to changing climate in western boreal North America
505 using a Multivariate Adaptive Regression Splines (MARS) approach. *Global Change*
506 *Biology*, 15(3). <https://doi.org/10.1111/j.1365-2486.2008.01679.x>
- 507 Bell, B., Hersbach, H., Simmons, A., Berrisford, P., Dahlgren, P., Horányi, A., et al. (2021). The
508 ERA5 global reanalysis: Preliminary extension to 1950. *Quarterly Journal of the Royal*
509 *Meteorological Society*, 147(741), 4186–4227. <https://doi.org/10.1002/qj.4174>
- 510 Bjorkman, A. D., Elmendorf, S. C., Beamish, A. L., Vellend, M., & Henry, G. H. R. (2015).
511 Contrasting effects of warming and increased snowfall on Arctic tundra plant phenology
512 over the past two decades. *Global Change Biology*, 21(12), 4651–4661.
513 <https://doi.org/10.1111/gcb.13051>
- 514 Boser, B. E., Guyon, I. M., & Vapnik, V. N. (1992). Training algorithm for optimal margin
515 classifiers. In *Proceedings of the Fifth Annual ACM Workshop on Computational Learning*
516 *Theory*. <https://doi.org/10.1145/130385.130401>
- 517 Braham, R. R., & Dungey, M. J. (1984). Quantitative Estimates of the Effect of Lake-Michigan
518 on Snowfall. *Journal of Climate and Applied Meteorology*, 23(6), 940–949.
519 [https://doi.org/10.1175/1520-0450\(1984\)023<0940:Qeoteo>2.0.Co;2](https://doi.org/10.1175/1520-0450(1984)023<0940:Qeoteo>2.0.Co;2)
- 520 Breiman, L. (2001). Random forests. *Machine Learning*, 45(1).
521 <https://doi.org/10.1023/A:1010933404324>
- 522 Budikova, D. (2012). Northern Hemisphere Climate Variability: Character, Forcing
523 Mechanisms, and Significance of the North Atlantic/Arctic Oscillation. *Geography*
524 *Compass*. <https://doi.org/10.1111/j.1749-8198.2012.00498.x>
- 525 Budikova, D., Ford, T. W., & Wright, J. D. (2022). Characterizing winter season severity in the
526 Midwest United States, part II: Interannual variability. *International Journal of*
527 *Climatology*, 42(6). <https://doi.org/10.1002/joc.7429>
- 528 Chantry, M., Christensen, H., Dueben, P., & Palmer, T. (2021). Opportunities and challenges for
529 machine learning in weather and climate modelling: Hard, medium and soft AI.
530 *Philosophical Transactions of the Royal Society A: Mathematical, Physical and*
531 *Engineering Sciences*, 379(2194). <https://doi.org/10.1098/rsta.2020.0083>
- 532 Chen, J., & Kumar, P. (2002). Role of terrestrial hydrologic memory in modulating ENSO
533 impacts in North America. *Journal of Climate*, 15(24). [https://doi.org/10.1175/1520-0442\(2003\)015<3569:ROTHMI>2.0.CO;2](https://doi.org/10.1175/1520-0442(2003)015<3569:ROTHMI>2.0.CO;2)
- 534
- 535 Chen, S., & Song, L. (2018). Impact of the Winter North Pacific Oscillation on the Surface Air
536 Temperature over Eurasia and North America: Sensitivity to the Index Definition. *Advances*
537 *in Atmospheric Sciences*, 35(6). <https://doi.org/10.1007/s00376-017-7111-5>
- 538 Chiodi, A. M., Potter, B. E., & Larkin, N. K. (2021). Multi-Decadal Change in Western US
539 Nighttime Vapor Pressure Deficit. *Geophysical Research Letters*, 48(15).
540 <https://doi.org/10.1029/2021GL092830>

541 Chipman, H. A., George, E. I., & McCulloch, R. E. (2012). BART: Bayesian additive regression
542 trees. *Annals of Applied Statistics*, 6(1). <https://doi.org/10.1214/09-AOAS285>

543 Choubin, B., Borji, M., Mosavi, A., Sajedi-Hosseini, F., Singh, V. P., & Shamshirband, S.
544 (2019). Snow avalanche hazard prediction using machine learning methods. *Journal of*
545 *Hydrology*, 577. <https://doi.org/10.1016/j.jhydrol.2019.123929>

546 Clark, C. A., Elless, T. J., Lyza, A. W., Ganesh-Babu, B., Koning, D. M., Carne, A. R., et al.
547 (2016). Spatiotemporal snowfall variability in the Lake Michigan Region: How is warming
548 affecting wintertime snowfall? *Journal of Applied Meteorology and Climatology*, 55(8).
549 <https://doi.org/10.1175/JAMC-D-15-0285.1>

550 Ford, T. W., Budikova, D., & Wright, J. D. (2021). Characterizing winter season severity in the
551 Midwest United States, Part I: Climatology and recent trends. *International Journal of*
552 *Climatology*. <https://doi.org/10.1002/joc.7431>

553 Francis, J. A., & Vavrus, S. J. (2012). Evidence linking Arctic amplification to extreme weather
554 in mid-latitudes. *Geophysical Research Letters*, 39(6).
555 <https://doi.org/10.1029/2012GL051000>

556 Friedman, J. H. (1991). Multivariate Adaptive Regression Splines. *The Annals of Statistics*,
557 19(1), 1–141.

558 Friedman, Jerome H. (2001). Greedy function approximation: A gradient boosting machine.
559 *Annals of Statistics*, 29(5). <https://doi.org/10.1214/aos/1013203451>

560 Ghatak, D., Gong, G., & Frei, A. (2010). North American temperature, snowfall, and snow-
561 Depth response to winter climate modes. *Journal of Climate*, 23(9).
562 <https://doi.org/10.1175/2009JCLI3050.1>

563 Gianola, D., Okut, H., Weigel, K. A., & Rosa, G. J. M. (2011). Predicting complex quantitative
564 traits with Bayesian neural networks: A case study with Jersey cows and wheat. *BMC*
565 *Genetics*, 12. <https://doi.org/10.1186/1471-2156-12-87>

566 Gibson, P. B., Chapman, W. E., Altinok, A., Delle Monache, L., DeFlorio, M. J., & Waliser, D.
567 E. (2021). Training machine learning models on climate model output yields skillful
568 interpretable seasonal precipitation forecasts. *Communications Earth & Environment*, 2(1).
569 <https://doi.org/10.1038/s43247-021-00225-4>

570 Grömping, U. (2009). Variable importance assessment in regression: Linear regression versus
571 random forest. *American Statistician*, 63(4). <https://doi.org/10.1198/tast.2009.08199>

572 Gutowski, W. J., Ullrich, P. A., Hall, A., Leung, L. R., O'Brien, T. A., Patricola, C. M., et al.
573 (2021). The ongoing need for high-resolution regional climate models: Process
574 understanding and stakeholder information. *Bulletin of the American Meteorological*
575 *Society*, 101(5). <https://doi.org/10.1175/BAMS-D-19-0113.1>

576 Ham, Y. G., Kim, J. H., & Luo, J. J. (2019). Deep learning for multi-year ENSO forecasts.
577 *Nature*, 573(7775). <https://doi.org/10.1038/s41586-019-1559-7>

578 Hartnett, J. J., Collins, J. M., Baxter, M. A., & Chambers, D. P. (2014). Spatiotemporal Snowfall
579 Trends in Central New York. *Journal of Applied Meteorology and Climatology*, 53(12),
580 2685–2697. <https://doi.org/10.1175/Jamc-D-14-0084.1>

581 Hill, J. D. (1971). *Snow squalls in the lee of Lakes Erie and Ontario*.

582 Hong, S. Y., Dudhia, J., & Chen, S. H. (2004). A revised approach to ice microphysical
583 processes for the bulk parameterization of clouds and precipitation. *Monthly Weather*
584 *Review*, 132(1). [https://doi.org/10.1175/1520-0493\(2004\)132<0103:ARATIM>2.0.CO;2](https://doi.org/10.1175/1520-0493(2004)132<0103:ARATIM>2.0.CO;2)

585 Kluver, D., & Leathers, D. (2015). Winter snowfall prediction in the United States using multiple
586 discriminant analysis. *International Journal of Climatology*, 35(8), 2003–2018.

587 Kolka, R. K., Giardina, C. P., McClure, J. D., Mayer, A., & Jurgensen, M. F. (2010). Partitioning
588 hydrologic contributions to an “old-growth” riparian area in the Huron Mountains of
589 Michigan, USA. *Ecohydrology*, 3(3). <https://doi.org/10.1002/eco.112>

590 Kuhn, M. (2008). Building predictive models in R using the caret package. *Journal of Statistical*
591 *Software*, 28(5). <https://doi.org/10.18637/jss.v028.i05>

592 Kunkel, K E, Ensor, L., Palecki, M., Easterling, D., Robinson, D., Hubbard, K. G., & Redmond,
593 K. (2009). A new look at lake-effect snowfall trends in the Laurentian Great Lakes using a
594 temporally homogeneous data set. *Journal of Great Lakes Research*, 35(1), 23–29.

595 Kunkel, Kenneth E., Westcott, N. E., & Kristovich, D. A. R. (2002). Assessment of potential
596 effects of climate change on heavy lake-effect snowstorms near Lake Erie. *Journal of Great*
597 *Lakes Research*, 28(4). [https://doi.org/10.1016/S0380-1330\(02\)70603-5](https://doi.org/10.1016/S0380-1330(02)70603-5)

598 Leathers, D. J., Yarnal, B., & Palecki, M. A. (1991). The Pacific/North American Teleconnection
599 Pattern and United States Climate. Part I: Regional Temperature and Precipitation
600 Associations. *Journal of Climate*, 4(5). [https://doi.org/10.1175/1520-](https://doi.org/10.1175/1520-0442(1991)004<0517:tpatpa>2.0.co;2)
601 [0442\(1991\)004<0517:tpatpa>2.0.co;2](https://doi.org/10.1175/1520-0442(1991)004<0517:tpatpa>2.0.co;2)

602 Li, X., Hu, Z. Z., Liang, P., & Zhu, J. (2019). Contrastive influence of ENSO and PNA on
603 variability and predictability of north American winter precipitation. *Journal of Climate*,
604 32(19). <https://doi.org/10.1175/JCLI-D-19-0033.1>

605 Mantua, N. J., Hare, S. R., Zhang, Y., Wallace, J. M., & Francis, R. C. (1997). A Pacific
606 Interdecadal Climate Oscillation with Impacts on Salmon Production. *Bulletin of the*
607 *American Meteorological Society*, 78(6). [https://doi.org/10.1175/1520-](https://doi.org/10.1175/1520-0477(1997)078<1069:APICOW>2.0.CO;2)
608 [0477\(1997\)078<1069:APICOW>2.0.CO;2](https://doi.org/10.1175/1520-0477(1997)078<1069:APICOW>2.0.CO;2)

609 Marshall, J., Kushnir, Y., Battisti, D., Chang, P., Czaja, A., Dickson, R., et al. (2001). North
610 Atlantic climate variability: Phenomena, impacts and mechanisms. *International Journal of*
611 *Climatology*, 21(15). <https://doi.org/10.1002/joc.693>

612 Meng, L., & Ma, Y. (2021). On the relationship of lake-effect snowfall and teleconnections in
613 the Lower Peninsula of Michigan, USA. *Journal of Great Lakes Research*, 47(1).
614 <https://doi.org/10.1016/j.jglr.2020.11.013>

615 Meng, L., Ayon, B. D., Koirala, N., & Baker, K. M. (2021). Inter-annual Variability of Snowfall
616 in the Lower Peninsula of Michigan. *Frontiers in Water*, 3.
617 <https://doi.org/10.3389/frwa.2021.746354>

618 Molnar, C., Casalicchio, G., & Bischl, B. (2020). Interpretable Machine Learning – A Brief
619 History, State-of-the-Art and Challenges. In *Communications in Computer and Information*
620 *Science* (Vol. 1323). https://doi.org/10.1007/978-3-030-65965-3_28

621 Nayak, M. A., & Ghosh, S. (2013). Prediction of extreme rainfall event using weather pattern
622 recognition and support vector machine classifier. *Theoretical and Applied Climatology*,
623 114(3–4). <https://doi.org/10.1007/s00704-013-0867-3>

624 Nelder, J. A., & Wedderburn, R. W. M. (1972). Generalized Linear Models. *Journal of the Royal*
625 *Statistical Society. Series A (General)*, 135(3), 370–384.

626 Newman, M., Alexander, M. A., Ault, T. R., Cobb, K. M., Deser, C., di Lorenzo, E., et al.
627 (2016). The Pacific decadal oscillation, revisited. *Journal of Climate*, 29(12).
628 <https://doi.org/10.1175/JCLI-D-15-0508.1>

629 Nguyen, D., & Widrow, B. (1990). Improving the learning speed of 2-layer neural networks by
630 choosing initial values of the adaptive weights. In *IJCNN. International Joint Conference*
631 *on Neural Networks*. <https://doi.org/10.1109/ijcnn.1990.137819>

632 Niziol, T. A. (1987). Operational Forecasting of Lake Effect Snowfall in Western and Central
633 New York. *Weather and Forecasting*, 2(4). [https://doi.org/10.1175/1520-](https://doi.org/10.1175/1520-0434(1987)002<0310:ofoles>2.0.co;2)
634 0434(1987)002<0310:ofoles>2.0.co;2

635 Notaro, M., Zarrin, A., Vavrus, S., & Bennington, V. (2013). Simulation of Heavy Lake-Effect
636 Snowstorms across the Great Lakes Basin by RegCM4: Synoptic Climatology and
637 Variability. *Monthly Weather Review*, 141(6), 1990–2014.

638 Novick, K. A., Ficklin, D. L., Stoy, P. C., Williams, C. A., Bohrer, G., Oishi, A. C., et al. (2016).
639 The increasing importance of atmospheric demand for ecosystem water and carbon fluxes.
640 *Nature Climate Change*, 6(11). <https://doi.org/10.1038/nclimate3114>

641 O’Gorman, P. A., & Dwyer, J. G. (2018). Using Machine Learning to Parameterize Moist
642 Convection: Potential for Modeling of Climate, Climate Change, and Extreme Events.
643 *Journal of Advances in Modeling Earth Systems*, 10(10).
644 <https://doi.org/10.1029/2018ms001351>

645 Pettersen, C., Kulie, M. S., Bliven, L. F., Merrelli, A. J., Petersen, W. A., Wagner, T. J., et al.
646 (2020). A Composite Analysis of Snowfall Modes from Four Winter Seasons in Marquette,
647 Michigan. *Journal of Applied Meteorology and Climatology*, 103–124.
648 <https://doi.org/10.1175/JAMC-D-19>

649 Quante, L., Willner, S. N., Middelani, R., & Levermann, A. (2021). Regions of intensification
650 of extreme snowfall under future warming. *Scientific Reports*, 11(1).
651 <https://doi.org/10.1038/s41598-021-95979-4>

652 Reddy, B. S. N., Pramada, S. K., & Roshni, T. (2021). Monthly surface runoff prediction using
653 artificial intelligence: A study from a tropical climate river basin. *Journal of Earth System*
654 *Science*, 130(1). <https://doi.org/10.1007/s12040-020-01508-8>

655 Robertson, A. W., Kumar, A., Peña, M., & Vitart, F. (2015). Improving and promoting
656 subseasonal to seasonal prediction. In *Bulletin of the American Meteorological Society*
657 (Vol. 96). <https://doi.org/10.1175/BAMS-D-14-00139.1>

658 Sasieni, P. (1992). Generalized additive models. T. J. Hastie and R. J. Tibshirani, Chapman and
659 Hall, London, 1990. No. of Pages: xv + 335. Price: £25. ISBN: 0-412-34390-8. *Statistics in*
660 *Medicine*, 11(7). <https://doi.org/10.1002/sim.4780110717>

661 Sauter, T., Weitzenkamp, B., & Schneider, C. (2010). Spatio-temporal prediction of snow cover
662 in the Black Forest mountain range using remote sensing and a recurrent neural network.
663 *International Journal of Climatology*, 30(15). <https://doi.org/10.1002/joc.2043>

664 Schneider, T., Lan, S., Stuart, A., & Teixeira, J. (2017). Earth System Modeling 2.0: A Blueprint
665 for Models That Learn From Observations and Targeted High-Resolution Simulations.
666 *Geophysical Research Letters*, 44(24). <https://doi.org/10.1002/2017GL076101>

667 Shi, Q., & Xue, P. (2019). Impact of Lake Surface Temperature Variations on Lake Effect Snow
668 Over the Great Lakes Region. *Journal of Geophysical Research: Atmospheres*, 124(23).
669 <https://doi.org/10.1029/2019JD031261>

670 Sillmann, J., Thorarindottir, T., Keenlyside, N., Schaller, N., Alexander, L. v., Hegerl, G., et al.
671 (2017). Understanding, modeling and predicting weather and climate extremes: Challenges
672 and opportunities. *Weather and Climate Extremes*.
673 <https://doi.org/10.1016/j.wace.2017.10.003>

674 Smith, S. R., & O’Brien, J. J. (2001). Regional snowfall distributions associated with ENSO:
675 Implications for seasonal forecasting. *Bulletin of the American Meteorological Society*,
676 82(6), 1179–1191. [https://doi.org/10.1175/1520-](https://doi.org/10.1175/1520-0477(2001)082<1179:Rsdawe>2.3.Co;2)
677 0477(2001)082<1179:Rsdawe>2.3.Co;2

678 Suriano, Z. J., & Leathers, D. J. (2017). Synoptic climatology of lake-effect snowfall conditions
679 in the eastern Great Lakes region. *International Journal of Climatology*, 37(12), 4377–
680 4389. <https://doi.org/10.1002/joc.5093>

681 Trenberth, K. E., & Guillemot, C. J. (1996). Physical processes involved in the 1988 drought and
682 1993 floods in north America. *Journal of Climate*, 9(6). [https://doi.org/10.1175/1520-
683 0442\(1996\)009<1288:PPIITD>2.0.CO;2](https://doi.org/10.1175/1520-0442(1996)009<1288:PPIITD>2.0.CO;2)

684 Trenberth, K. E., & Hurrell, J. W. (1994). Decadal atmosphere-ocean variations in the Pacific.
685 *Climate Dynamics*, 9(6). <https://doi.org/10.1007/BF00204745>

686 Tripathi, S., Srinivas, V. v., & Nanjundiah, R. S. (2006). Downscaling of precipitation for
687 climate change scenarios: A support vector machine approach. *Journal of Hydrology*,
688 330(3–4). <https://doi.org/10.1016/j.jhydrol.2006.04.030>

689 Wei, W., Yan, Z., Tong, X., Han, Z., Ma, M., Yu, S., & Xia, J. (2022). Seasonal prediction of
690 summer extreme precipitation over the Yangtze River based on random forest. *Weather and
691 Climate Extremes*, 37, 100477. <https://doi.org/10.1016/j.wace.2022.100477>

692 Zhou, Q., Li, D., Xia, S., Chen, Z., Wang, B., & Wu, J. (2021). Plant–rodent interactions after a
693 heavy snowfall decrease plant regeneration and soil carbon emission in an old-growth
694 forest. *Forest Ecosystems*, 8(1). <https://doi.org/10.1186/s40663-021-00310-2>

695 Zhu, L., & Aguilera, P. (2021). Evaluating Variations in Tropical Cyclone Precipitation in
696 Eastern Mexico Using Machine Learning Techniques. *Journal of Geophysical Research:
697 Atmospheres*, 126(7). <https://doi.org/10.1029/2021JD034604>

698 Zwiers, F. W., Alexander, L. v., Hegerl, G. C., Knutson, T. R., Kossin, J. P., Naveau, P., et al.
699 (2013). Climate Extremes: Challenges in Estimating and Understanding Recent Changes in
700 the Frequency and Intensity of Extreme Climate and Weather Events. In *Climate Science
701 for Serving Society*. https://doi.org/10.1007/978-94-007-6692-1_13
702
703
704